The Astrophysical Journal, 775:22 (10pp), 2013 September 20 doi:10.1088/0004-637X/775/1/22

A STATISTICAL STUDY OF CORONAL ACTIVE EVENTS IN THE NORTH POLAR REGION

Nobuharu Sako[1,2], Masumi Shimojo[1,2], Tetsuya Watanabe[1,2], and Takashi Sekii[1,2]
[1] The Graduate University for Advanced Studies (SOKENDAI), Mitaka, Tokyo 181-8588, Japan; sako@solar.mtk.nao.ac.jp
[2] National Astronomical Observatory of Japan (NAOJ), Mitaka, Tokyo 181-8588, Japan
Received 2012 December 17; accepted 2013 July 17; published 2013 August 30

ABSTRACT

In order to study the relationship between characteristics of polar coronal active events and the magnetic environment in which such events take place, we analyze 526 X-ray jets and 1256 transient brightenings in the polar regions and in regions around the equatorial limbs. We calculate the occurrence rates of these polar coronal active events as a function of distance from the boundary of coronal holes, and find that most events in the polar quiet regions occur adjacent to and equatorward of the coronal hole boundaries, while events in the polar coronal holes occur uniformly within them. Based primarily on the background intensity, we define three categories of regions that produce activity: polar coronal holes, coronal hole boundary regions, and polar quiet regions. We then investigate the properties of the events produced in these regions. We find no significant differences in their characteristics, for example, length and lifetime, but there are differences in the occurrence rates. The mean occurrence rate of X-ray jets around the boundaries of coronal holes is higher than that in the polar quiet regions, equatorial quiet regions, and polar coronal holes. Furthermore, the mean occurrence rate of transient brightenings is also higher in these regions. We make comparison with the occurrence rates of emerging and canceling magnetic fields in the photosphere reported in previous studies, and find that they do not agree with the occurrence rates of transient brightenings found in this study.

Key words: Sun: activity – Sun: corona

1. INTRODUCTION

Dynamic events are commonly observed in the solar corona, and their frequency is often used as a measure of the level of coronal activity. Observations by the soft X-ray telescope (SXT; Tsuneta et al. 1991) on board the *Yohkoh* satellite (Ogawara et al. 1991) revealed that many small flares, named "transient brightenings," are constantly occurring in the corona. Shimizu et al. (2002) showed that half of these transient brightenings appeared above emerging flux regions, while Kotoku et al. (2007) discussed the possibility that transient brightenings associated with X-ray bright points (XBPs) are related with magnetic flux cancellation. These results suggest that we should consider both flux emergence and cancellation as photospheric counterparts of transient brightenings.

X-ray jets are also commonly observed in the solar corona (Shibata et al. 1992). These jets are characterized by thin elongated structures in X-rays. They are also associated with small flares, and people generally think that this small flare is a kind of a transient brightening. Some authors have reported that X-ray jets occur in photospheric regions where magnetic fields are emerging or canceling (e.g., Canfield et al. 1996; Shimojo et al. 1998; Chifor et al. 2008; Huang et al. 2012). The magnetic and morphological evolution of X-ray jets is explained well by MHD simulations and theoretical modeling of magnetic reconnection (e.g., Yokoyama & Shibata 1995, 1996; Nishizuka et al. 2008; Moreno-Insertis et al. 2008).

Shimojo et al. (1996) carried out a statistical study of 100 X-ray jets observed by *Yohkoh*/SXT, and showed that the frequency of X-ray jets in coronal holes is lower than that in active regions. However, recent X-ray observations have revealed that X-ray jets in polar coronal holes are occurring more frequently than previously thought (Cirtain et al. 2007). Savcheva et al. (2007) showed that the typical length scale and lifetime of X-ray jets in PCHs were smaller than those reported by Shimojo et al. (1996). It has therefore been suggested that the spatial and temporal resolution of *Yohkoh*/SXT was not enough to detect polar X-ray jets, and that the occurrence rate of X-ray jets in coronal holes was underestimated. Furthermore, recent studies have suggested that jets in coronal holes appear more frequently than in quiet regions, and that this is true not only in coronal holes themselves, but also around their boundaries (Subramanian et al. 2010; Yang et al. 2011).

The relationship between coronal activity in the polar regions and the structure of the magnetic field is not yet well understood. In order to study this relationship, we have identified X-ray jets and transient brightenings in the polar regions (including both coronal holes and quiet Sun), using images taken by the X-Ray Telescope (XRT; Golub et al. 2007; Kano et al. 2008) on board the *Hinode* satellite. We then statistically investigate the characteristics of these X-ray jets and transient brightenings, and examine the regional differences between these phenomena. In Section 2, we describe the observations and our detection method. In Section 3, we discuss the characteristics of the X-ray jets and transient brightenings and the differences between regions.

2. OBSERVATIONS AND DATA ANALYSIS

2.1. Observations

In 2007 September, the *Hinode* satellite (Kosugi et al. 2007) observed regions around the north pole for 3 weeks. X-ray images were taken by XRT in the period of September 5–22. We obtained 35 sets of observations and the average duration of each observation was about 6 hr. The temporal cadence of the observations was 80 s for some data sets and 120 s for the others. The XRT plate scale was $1''.028$ pixel^{-1}, and the field of view was $1053''$(E–W) $\times$ $395''$(N–S). The exposure time for the observations was 16 s.

In order to detect X-ray jets and transient brightenings even if they show only weak X-ray intensity enhancements, we used the thinnest of the XRT filters: Al-poly. The Al-poly

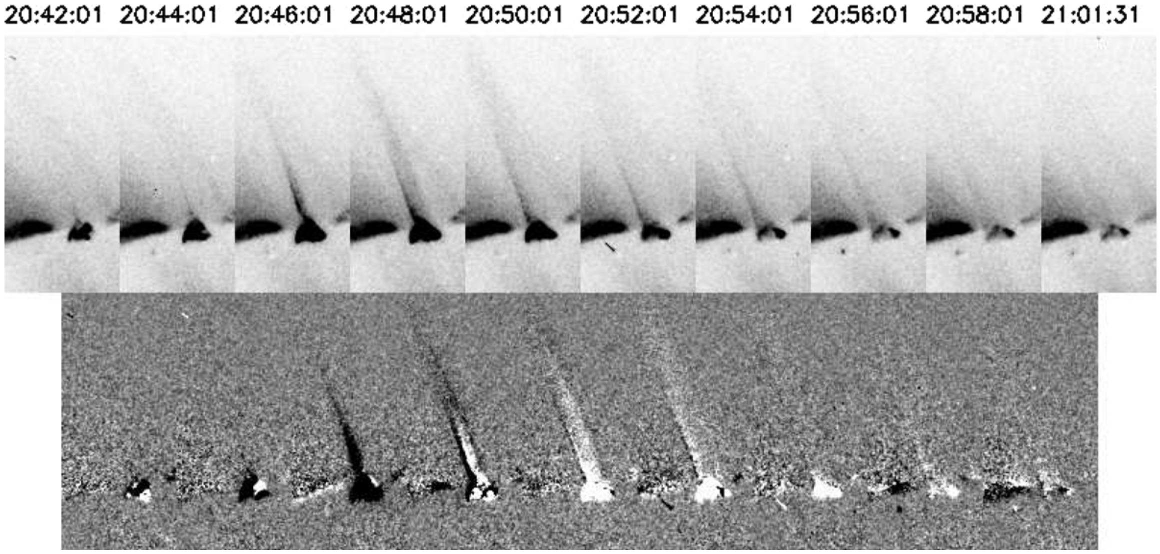

Figure 1. Example of a polar X-ray jet. The field of view in each panel is 82″× 185″. An X-ray jet occurred on 2007 September 5, near the north pole. Upper panels show X-ray images, while lower panels show running difference images.

filter has extended temperature sensitivity down to plasma at 1 MK (Narukage et al. 2011). To investigate differences in the characteristics of these phenomena around the pole and equator, we also used X-ray images that contained the equatorial limbs within the field of view in 2007 September and November. The total observing time for the data we analyzed is about 66 hr. The spatial and temporal resolution and the XRT filter used for the equatorial limb observations are similar to those of the polar images, but the field of view was 527″× 527″and the time cadence was 80 s. We calibrated the X-ray intensity and instrument pointing using "xrt_prep.pro" and "xrt_jitter.pro" in the Solar Software package (SSWidl; Freeland & Handy 1998).

2.2. Detection

2.2.1. Detection of X-Ray Jets by Visual Inspection

Most X-ray jets have two prominent structures. The first is that they are thin structures, and this structure elongates over time. The X-ray intensity distribution along the structure also shows an exponential decrease toward the apex (Shibata et al. 1992). The second feature is that brightenings near the base of the thin structure, an XBP or a small loop system, usually exist prior to the event (Shimojo et al. 1996), and they brighten when the thin structure of the jet appears. We call these brightenings "footpoint flares." Using the footpoint flares as markers, we define X-ray jets as follows.

1. A thin structure, which was not observed before, appears when a footpoint flare initiates and then elongates with time.
2. The ratio of the length to the width of the thin structure is more than 2 at the maximum elongation.

We visually inspected the data sets to search for events that satisfy both these criteria. Running difference images (see Figure 1) were used to detect as many small and short-lived X-ray jets as possible (Savcheva et al. 2007). Applying this method, we successfully detected 844 events around the north polar regions and 55 events in the equatorial quiet regions.

2.2.2. Automatic Detection of Transient Brightenings

We also studied another kind of dynamic coronal event: transient brightenings. Schemes to automatically detect transient

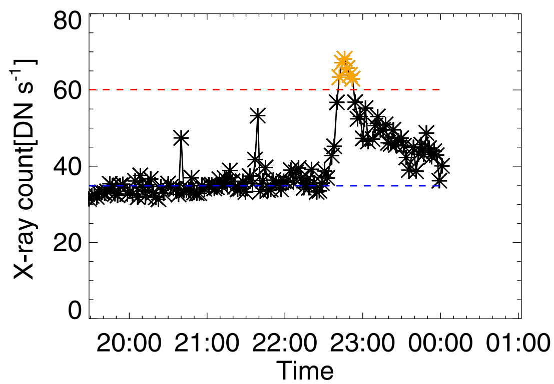

Figure 2. Sample time profile of the X-ray counts in a macro-pixel. The blue and red dashed lines indicate three times the standard deviation and the background level, respectively. The orange asterisks show the candidates for transient brightenings.

brightenings have already been developed (e.g., Shimizu 1995; Aschwanden et al. 2000; Subramanian et al. 2010). We made some improvements to these methods and applied them to our XRT data sets. Our automatic detection scheme is as follows.

2.2.2.1. Preparation of macro-pixel images. To improve the signal-to-noise ratio in the images, we sum the X-ray counts in 4 × 4 pixels to obtain macro-pixel images. We then only use the macro-pixels that are located fully inside the solar X-ray limb. The spatial resolution of these macro-pixel images is 4″.098.

2.2.2.2. Detection of X-ray enhancement. To detect the X-ray enhancement in a brightening, we use the temporal intensity profile of the X-ray counts in each macro-pixel. First, we compute the mean count level in each macro-pixel over the observation period (about 6 hr). Then we select counts that are smaller than this average, and assume that they represent the background. We then compute the "average background level" by averaging the background X-ray counts. Next, we derive the standard deviation of the X-ray count in each macro-pixel. If the enhancement above the average background level exceeds three times the standard deviation, we identify the macro-pixel as a "candidate pixel" for a transient brightening (see Figure 2). By repeating this procedure for the entire data set, we make a

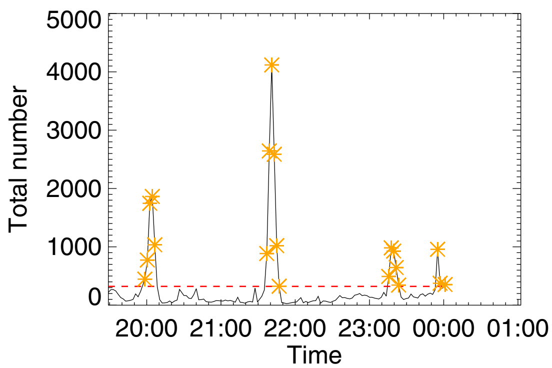

Figure 3. Time profile of the total number of candidate pixels in an on-disk macro-pixel. The red dashed line indicates the threshold value for SAA. The orange asterisks show the SAA periods.

"candidate map," showing the times and positions of candidate pixels.

Highly energized particles passing through the orbit of *Hinode* sometimes also produce X-ray enhancements. To eliminate these events, we add two more criteria. The purpose of the first is to exclude events produced by high-energy particles in the South Atlantic Anomaly (SAA). When *Hinode* enters the SAA, the X-ray count rates increase in many macro-pixels simultaneously (Figure 3). We define the SAA period as the period during which more than 3% of all the macro-pixels become "candidate pixels," and any candidates detected during the SAA period are ignored.

The second criterion is mainly for eliminating cosmic-ray events or those coming from the High Latitude Anomaly. If a candidate macro-pixel does not show the enhancement in three consecutive images, the candidate pixel is not identified as exhibiting a transient brightening.

2.2.2.3. Identification of transient brightenings as single events. Occasionally, the size of a transient brightening exceeds the size of the macro-pixel, leading to the X-ray enhancement taking place in more than one macro-pixel. To account for such events, our program identifies these brightenings as one event, provided the candidate pixels are located side by side. We also employ this criterion in the time domain. More precisely, if there are candidates in the same position in successive images, candidates in these pixels are identified as belonging to the same event.

2.2.2.4. Categorization of transient brightenings as with/without an associated X-ray jet. In order to compare X-ray jets with "pure" transient brightenings, we categorized them into those that are associated with an X-ray jet and those that are not. Transient brightenings with X-ray jets, which account for 4% of all the transient brightenings, are the ones whose position and timing are consistent with this association.

Under these criteria, we identified 3436 transient brightenings in the north polar regions and 257 in the equatorial quiet regions.

2.3. Derivation and Estimation of the Parameters of the Detected Events

2.3.1. Parameters for X-Ray Jets

In this study, we derive and estimate five parameters for the elongated thin structures and three parameters for the footpoint flares. The parameters characterizing the thin structures are length, lifetime, apparent velocity, width, and angle between the direction of elongation and the normal vector of the associated footpoint flare. The derived parameters are values projected on the image plane, of course, since XRT does not have the capability to observe the line-of-sight components of motion associated with the footpoint flares. For the footpoint flares, the area, total X-ray intensity, and thermal energy are derived. The length of the thin structures is measured, by visual inspection, between the apex of the structure and the footpoint flare at the time of the maximum of the X-ray counts. The lifetime of an X-ray jet is defined as the time interval between the time of its first appearance and the time of its disappearance. The width is defined as the diameter of the thin structure at its midpoint, when the height of the jet reaches its maximum. The apparent velocity of the X-ray jet is estimated by dividing the maximum length by the time interval between the time of its first appearance and the time it reaches its maximum length. The direction of the X-ray jets is also used for investigating the coronal magnetic fields.

In this study, the normal vector is defined at the center of the footpoint flare for reference. On the other hand, the X-ray jet's direction is defined as a vector starting from the center of the footpoint flare and ending at the apex of the X-ray jet. We measure the angles clockwise from the normal direction to the X-ray jet's direction, projected on the image plane, and use this as one of the parameters characterizing X-ray jets.

The area of a footpoint flare is defined as the area of the rectangle that circumscribes the footpoint flare. In this paper, the limb foreshortening effect is corrected by taking into account the latitude and longitude of the event. The total X-ray intensity of the footpoint flare is obtained by integrating the X-ray counts in the rectangular area at the time of its maximum and subtracting the background level. The background level is determined by the same method that we used for the automatic detection of transient brightenings. For the thermal energy of the footpoint flare, we assume that its temperature is 1 MK. This corresponds to the temperature of the peak of the XRT response curve for the Al-poly filter (Narukage et al. 2011). The depth of the footpoint flaring loop is assumed to be the same as the shorter side of the rectangle. The assumption of the plasma temperature is not entirely justified, but the thermal energy is only proportional to the temperature and therefore this rough estimation should not affect our results significantly.

2.3.2. Parameters for Transient Brightenings

In order to investigate the properties of the transient brightenings in each region, we derive four parameters for the candidate maps: the area, total X-ray intensity, lifetime, and thermal energy. The lifetime of a transient brightening is the duration from first appearance to disappearance of the brightening in the candidate pixels. The total X-ray intensity is the maximum of the integrated X-ray counts over the candidate pixels during the event. The area of the transient brightening is derived from the number of the candidate pixels at the peak time of the total X-ray count. Finally, we estimate the thermal energy of the transient brightening using the same method as applied for the footpoint flares.

3. RESULTS

3.1. Classification of the Polar Regions Based on X-Ray Intensity

In order to compare the characteristics of X-ray jets and transient brightenings in open and closed magnetic field regions, we first divide the polar regions into coronal holes and quiet

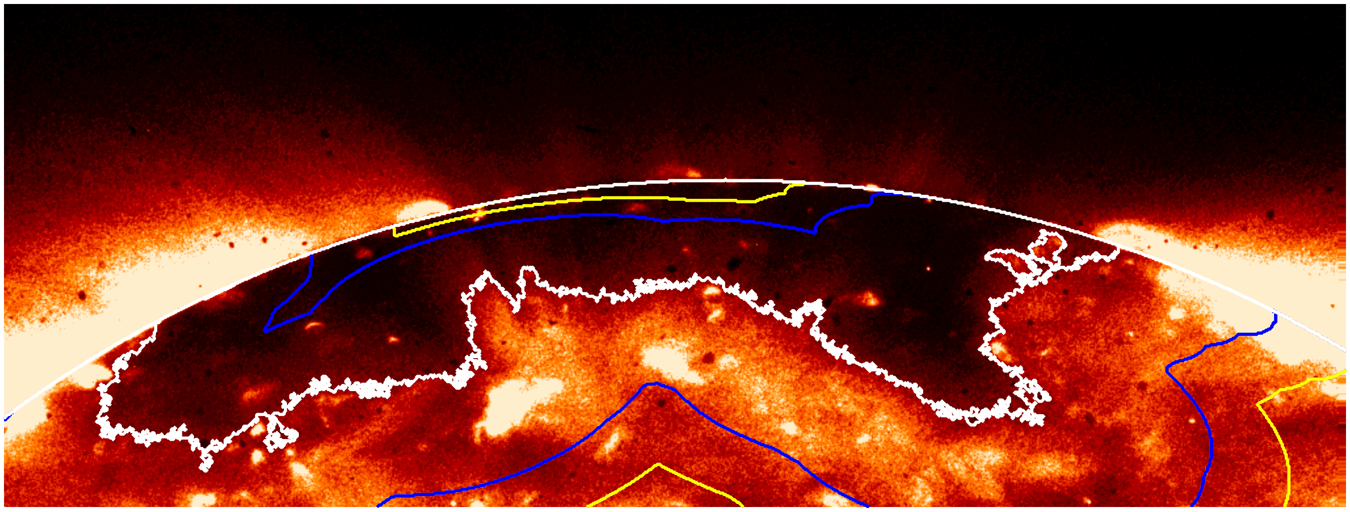

Figure 4. X-ray image on 2007 September 5 around the north pole. The white line shows the boundary of the coronal hole. The boundary between the CHB and the PQR is indicated by the blue line for X-ray jets and the yellow line for transient brightenings.

regions. By visual inspection of X-ray images, we choose an intensity threshold of 3.5 DN s^{-1} $pixel^{-1}$ to define the boundaries of the coronal holes (where DN is the data number). A region with an intensity less than the threshold is considered to be a coronal hole in this study (see Figure 4). Using this classification scheme, 467 X-ray jets are detected in the polar coronal holes, and 377 are detected in the polar quiet regions. The number of transient brightenings detected in the polar coronal holes reaches 1862 during our observations, and 1564 are detected in the polar quiet regions. All the events detected in regions near the equatorial limb fall into the quiet region classification.

3.2. Influence of the X-Ray Background Level on the Detection of Events

Because our X-ray jet/transient brightening detection method uses the contrast between the background level and X-ray intensity of the event, the background level could affect the efficiency of the event detection. In particular, we may tend to detect more events in regions with weaker background levels, such as coronal holes. In order to evaluate the influence of the background level on the performance of the detection method, we investigate the X-ray intensity of events in such regions, after subtracting the background level. Figures 5 and 6 show the frequencies of X-ray jets and transient brightenings plotted against the excess of their X-ray intensities. In Figure 5, for the X-ray jets, the excess of the X-ray intensity at the half of the jet's length is used, and in Figure 6, for the transient brightenings, the average excess of the X-ray intensity of the brightening is used. The error bars in the figures represent $\pm 1\sigma$ uncertainties, assuming a Poisson distribution for the number of events in each bin. Hereafter, the error bars in all the figures indicate $\pm 1\sigma$ Poisson errors.

Assuming that the inverse relationship between the frequency and excess of X-ray intensity is valid down to unobservable values, the positions of the peaks of the distributions suggest where the lower limits for a consistent use of our detection method might be. In Figure 5, for the X-ray jets, no significant difference in the peak positions is found and they are located at around 1 DN s^{-1} $pixel^{-1}$, while for the transient brightenings in Figure 6, the peak position in the polar coronal holes is lower than that in the polar and equatorial quiet regions, indicating

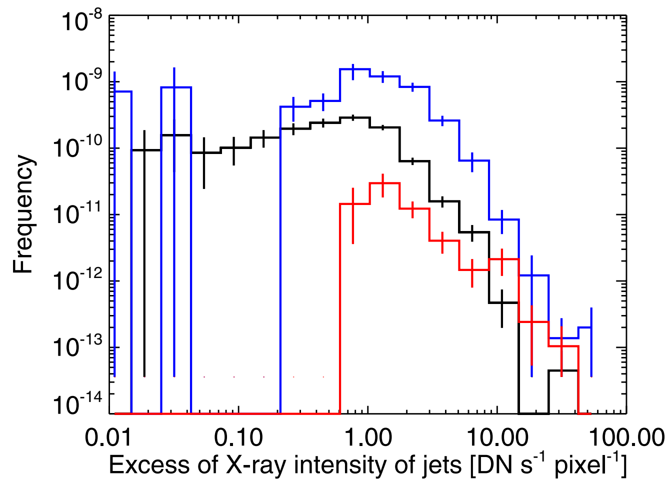

Figure 5. Frequency distributions of the X-ray jets. The black, blue, and red lines show X-ray jets occurring in the polar coronal holes, the polar quiet regions, and the equatorial quiet regions, respectively. The horizontal axis indicates the excess of the X-ray intensity of the thin structures and the vertical axis indicates the event number normalized by total area and duration of the observation.

that the background level is affecting the detection method. To avoid this possible bias due to the background levels, we set lower limits for the sample of events as follows: for X-ray jets, the value of 1 DN s^{-1} $pixel^{-1}$ is naturally adopted; and for transient brightenings, it is set to 10 DN s^{-1} $pixel^{-1}$, which is the peak position in the quiet regions. After rejecting events below these limits, the number of X-ray jets used in this study become 213 in the polar coronal holes, 265 in the polar quiet regions, and 48 in the equatorial quiet regions. The number of transient brightenings became 216 in the polar coronal holes, 958 in the polar quiet regions, and 82 in the equatorial quiet regions.

3.3. Occurrence Rate as a Function of the Distance from the Coronal Hole Boundary

In order to examine the spatial distribution of the events occurring in each region, we measured their distances from the coronal hole boundaries. We investigated the distribution of the occurrence rate as a function of the distance, that is,

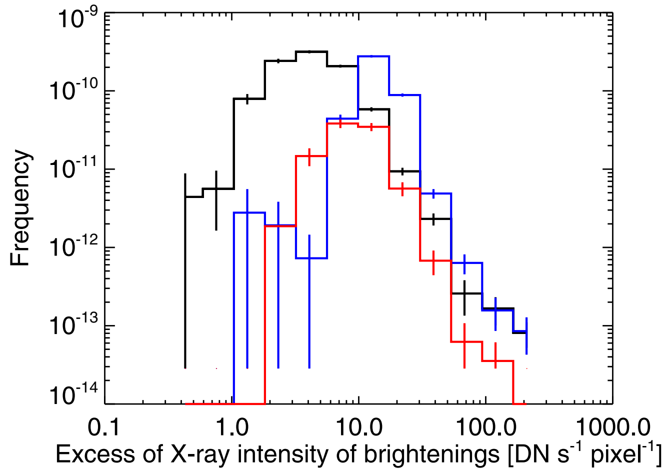

Figure 6. Frequency distributions of the transient brightenings. The black, blue, and red lines show transient brightenings in the polar coronal holes, the polar quiet regions, and the equatorial quiet regions, respectively.

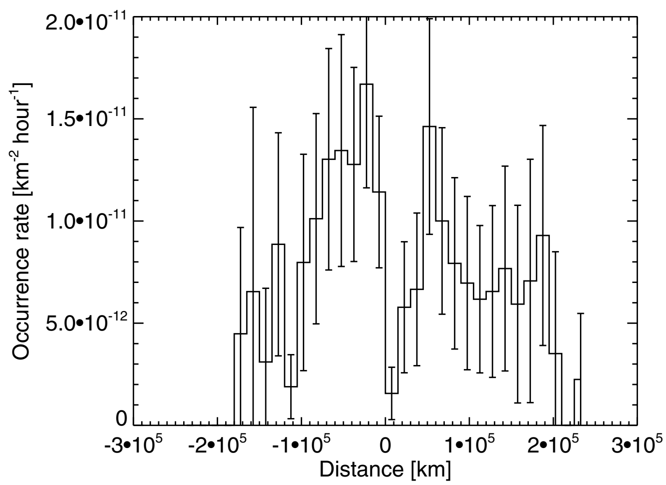

Figure 7. Occurrence rates of the X-ray jets as a function of the distance from the boundary of coronal holes. Zero is the position of the boundary of coronal holes. Negative values of distances indicate a location in the polar quiet regions and positive values indicate a location in the polar coronal holes.

the minimum of the distances measured from the locus of the boundary to the event position (Figures 7 and 8). The occurrence rate is the frequency of the events normalized by the time and area in each distance bin. Figure 7 shows that the frequency of X-ray jets is uniformly distributed in the polar coronal holes between the distance of 2×10^4 km and 2×10^5 km, and decreases from a distance of 2×10^5 km. The uncertainty of the distribution becomes large above 2×10^5 km because the observed areas, being close to the north pole, are very small. We found that the occurrence rates of X-ray jets in the polar quiet regions start to decrease rapidly at a distance of 10^5 km, and this cannot wholly be attributed to the observational uncertainties. Therefore, most of the X-ray jets in the polar quiet regions are concentrated within 10^5 km of the boundary. Note that there is a dip in the 0 to $+3 \times 10^4$ km distance bin. We have carefully checked our analysis method and found that it is a real feature. It probably reflects a difference in the physical environment just at the vicinity of the regions around the boundary of the coronal holes. We have, however, no simple explanation for this observation.

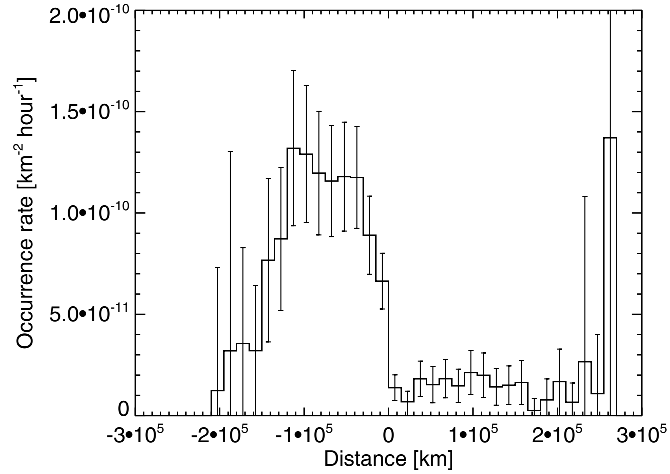

Figure 8. Same as Figure 7 but for the transient brightenings.

Figure 8 shows the distribution of transient brightenings as a function of the distance from the boundaries of the coronal holes. The distribution in the polar coronal holes is roughly uniform within a distance of 2×10^5 km. We also find that most of the transient brightenings in the polar quiet regions occur adjacent to and equatorward of the boundaries of the coronal holes. While the other properties are similar to those of the X-ray jets, the largest distance where the occurrence rates are high is somewhat larger in the polar quiet regions, and is estimated to be 1.5×10^5 km.

We also find some differences in the occurrence rates of the X-ray jets and transient brightenings in Figures 7 and 8. The ratio of the mean occurrence rate of the X-ray jets in the polar quiet regions to that in the polar coronal holes is about 2, while the same ratio for the transient brightenings is about 6. In coronal holes, a single magnetic polarity is dominant, and large-scale coronal loops may be created more often than they are in quiet regions with mixed polarities. Magnetic reconnection could tend to take place more often in large-scale coronal loops and produce X-ray jets.

To investigate the characteristics of X-ray jets and transient brightenings near the boundaries of coronal holes, we classify the polar areas into three regions. The "polar coronal hole (PCH)" is defined as the region where the X-ray intensity is lower than 3.5 DN s^{-1} pixel^{-1}. The "coronal hole boundary (CHB) region" is defined as the region where the X-ray intensity is higher than 3.5 DN s^{-1} pixel^{-1} and the distance to the boundaries of the coronal holes is less than 10^5 km for X-ray jets and 1.5×10^5 km for transient brightenings; and the "polar quiet region (PQR)" is defined as the region where the X-ray intensity is greater than 3.5 DN s^{-1} pixel^{-1} and the distance to the boundaries of the coronal holes is more than 10^5 km for X-ray jets and 1.5×10^5 km for transient brightenings. Based on these classifications, the number of X-ray jets in these three regions is 213 in the PCHs, 240 in the CHBs, and 25 in the PQRs. Also, the number of transient brightenings is 216 in the PCHs, 934 in the CHBs, and 24 in the PQRs. The sum of the events in the PCHs, CHBs, and PQRs is equal to the number of events in the complete sample in the polar region.

3.4. Daily Occurrence Rate of X-Ray Jets and Transient Brightenings

In order to study differences between the X-ray jets and transient brightenings that depend on the region observed, we compared the characteristics of these phenomena in the PCHs,

Table 1
The Daily Occurrence Rates of X-Ray Jets and Transient Brightenings

	PCH	CHB	PQR	EQR
X-ray jets (10^{-12} km^{-2} hr^{-1})	6.84 ± 0.54	12.5 ± 0.89	4.80 ± 1.09	4.52 ± 0.74
Transient brightenings (10^{-11} km^{-2} hr^{-1})	1.64 ± 0.12	11.4 ± 0.42	4.33 ± 1.15	4.11 ± 0.52

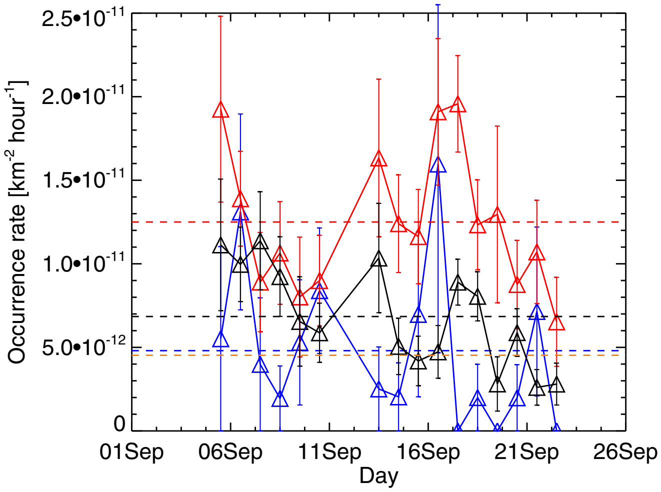

Figure 9. Temporal variations of daily occurrence rates of X-ray jets. The triangles joined by the solid lines are daily occurrence rates, while horizontal dashed lines are the mean values. The black, red, blue, and orange lines show the rates in the PCHs, CHBs, PQRs, and EQRs, respectively.

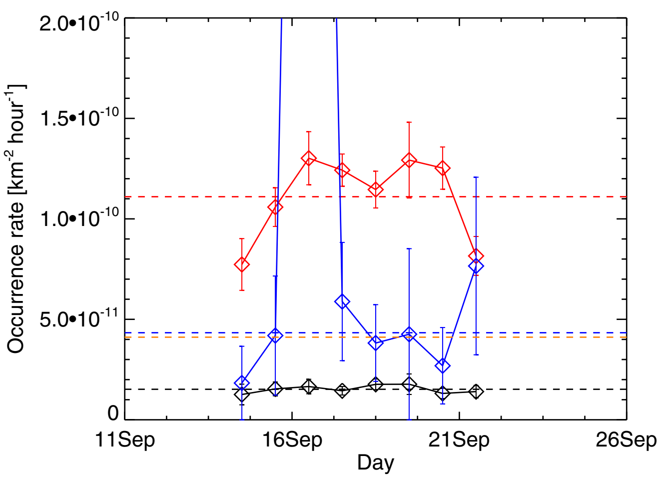

Figure 10. Temporal variations of daily occurrence rates of transient brightenings (diamonds). The dashed lines are mean values. The black, red, blue, and orange solid lines show distributions of transient brightenings in the PCHs, CHBs, PQRs, and EQRs, respectively.

CHBs, and PQRs. First, we compared the daily occurrence rates of these phenomena in each region.

Figure 9 shows the temporal variation of the daily occurrence rates of the X-ray jets in each region. The daily occurrence rate is the number of the events per day normalized by the area and the total observing time. The amount of variation is such that, in each region, the ratio of the maximum to the minimum is 3–8. The mean occurrence rate of the X-ray jets in the CHBs is two to three times larger than that in the PCHs, PQRs, and "equatorial quiet regions" (EQRs) (Table 1).

The temporal variation of the daily occurrence rates of the transient brightenings is shown in Figure 10. When we calculate the mean occurrence rate of the transient brightenings in the PQRs, we exclude the September 16 data because the area of the PQRs on that date is an order of magnitude less than the area on the other days. The mean daily occurrence rate of the transient brightenings in the CHBs is eight times more than that in the PCHs and three times more than that in the PQRs and EQRs (Table 1).

The period of our observational data covers half of the rotation period around the pole. The daily occurrence rates of the X-ray jets and transient brightenings in each region vary within the error bars. This result shows that these events do not have a longitudinal dependence.

3.5. Parameters of X-Ray Jets and Transient Brightenings

Tables 2 and 3 summarize our measured physical parameters, for example, the length and lifetime for the X-ray jets and transient brightenings, respectively. No significant differences exist between the regions producing the transient activity. Our results are also consistent with those reported by Savcheva et al. (2007).

3.6. Frequency Distributions as a Function of X-Ray Intensity

Figure 11 shows frequency distributions of the footpoint flares that are associated with X-ray jets. The power-law indices of the distributions are -1.78 ± 0.17 (PCHs), -1.75 ± 0.13 (CHBs), and -1.13 ± 0.09 (EQRs). Because only 25 X-ray jet events are detected in the PQRs, we cannot derive a power-law index for that region. The distributions in the PCHs and CHBs have indices steeper than that in the EQRs. Shimojo et al. (1996) showed that the power-law index of footpoint flares associated with X-ray jets is -1.2. In their study, about 70% of their samples are X-ray jets that occurred in active regions. The indices in quiet regions are therefore closer to those in active regions, rather than in PCHs and CHBs.

The frequency distributions for the transient brightenings are shown in Figure 12. The power-law indices are -2.12 ± 0.17 (PCHs), -2.03 ± 0.07 (CHBs), and -1.92 ± 0.08 (EQRs). We cannot derive the index for the PQRs because only 24 transient brightenings were detected there. The power-law indices are consistent with each other; the differences being within the error bars. Shimizu (1995) reported that the power-law index of transient brightenings in active regions is -1.4, and Aschwanden & Parnell (2002) reported that the power-law index of transient brightenings in EQRs is -1.74 ± 0.08. The power-law index in active regions is therefore flatter than that for other coronal regions.

3.7. Direction of X-Ray Jets

Hot plasma, created in an X-ray jet, flows along the coronal magnetic field. We can therefore investigate the structure of the polar magnetic fields from the X-ray jet's flow direction. Figure 13 shows histograms of the absolute values of the angle from the direction of the X-ray jets to the normal direction at the center of the footpoint flares. Most of the X-ray jets in the PCHs flow along the normal direction of the solar surface. This suggests that magnetic fields in PCHs are mostly radial. On the other hand, the erupting angles of the X-ray jets in the PQRs

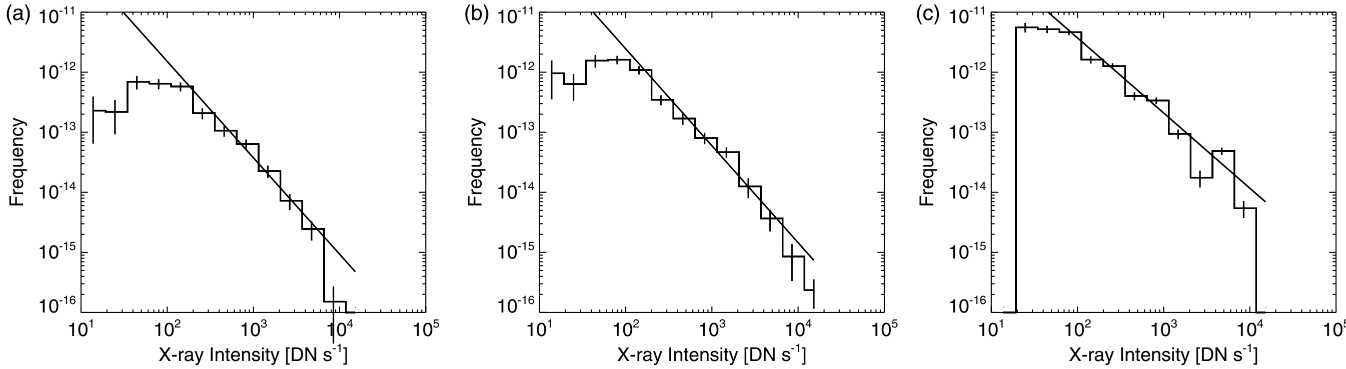

Figure 11. Frequency distributions as a function of the X-ray intensity of footpoint flares. The panels from (a) to (c) show frequency distributions in the PCHs, CHBs, and EQRs. The solid lines show least-square fits. Vertical axes indicate the X-ray intensity of footpoint flares normalized by the exposure time, total area, and duration of the observation.

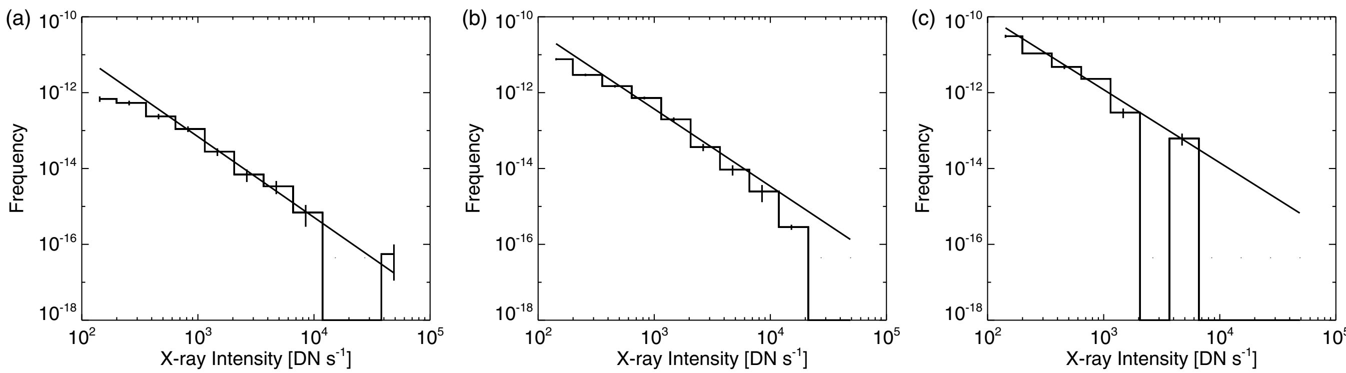

Figure 12. Same as Figure 11 but for transient brightenings.

Table 2
The X-Ray Jets Parameters

		PCH	CHB	PQR	EQR
Length (10^4 km)	Mean	2.63	2.96	2.84	2.64
	Range	0.44–16.2	0.62–9.19	0.76–10.8	0.56–9.72
Lifetime (minutes)	Mean	10	11	10	8
	Range	3–45	3–38	3–27	3–33
Velocity (km s^{-1})	Mean	181	173	164	177
	Range	23–811	30–615	43–611	15–538
Width (10^3 km)	Mean	4.07	4.42	4.15	3.54
	Range	0.76–13.1	0.76–12.7	1.52–12.2	1.52–7.76
Area (10^7 km^2)	Mean	3.26	3.79	3.36	2.47
	Range	0.92–16.6	0.46–27.8	0.92–11.1	0.92–6.95
Thermal energy (10^{25} erg)	Mean	7.27	8.72	6.13	8.29
	Range	0.36–65.5	0.30–185	0.71–30.6	0.59–58.8

Table 3
The Transient Brightenings Parameters

		PCH	CHB	PQR	EQR
Lifetime (minutes)	Mean	5	5	5	4
	Range	4–12	4–15	4–12	4–10
Area (10^7 km^2)	Mean	2.61	2.35	1.81	2.04
	Range	0.92–13.9	0.92–25.9	0.92–4.63	0.92–12.0
Thermal energy (10^{25} erg)	Mean	9.06	7.47	4.20	6.37
	Range	1.14–228	1.13–193	1.16–19.3	1.38–89.7

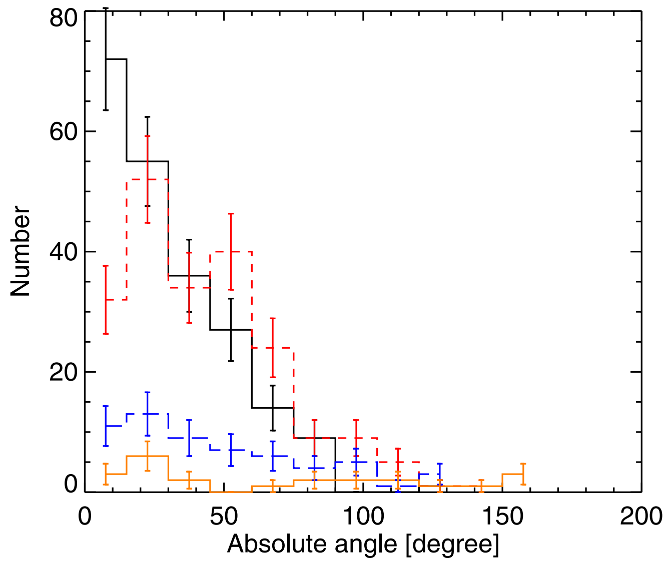

Figure 13. Histograms of the absolute angles between the direction of the X-ray jets and the normal directions of the footpoint flares. The black solid, red dashed, blue long-dashed, and orange solid lines are for the X-ray jets observed in the PCHs, CHBs, PQRs, and EQRs, respectively.

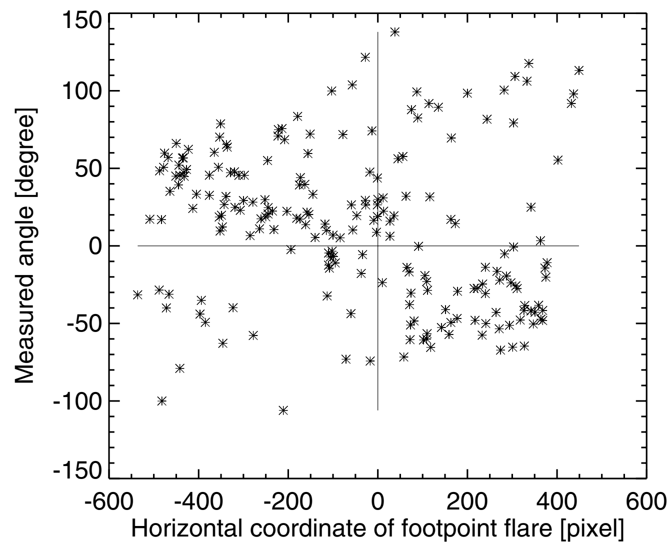

Figure 14. Scatter diagram of the horizontal (east–west) coordinates of footpoint flares and the clockwise-measured angles from the surface normal vector to the directions of X-ray jets.

and EQRs are rather uniformly distributed. These distributions indicate that magnetic elements are randomly oriented in quiet regions, in which closed magnetic fields would be preferentially created. Finally, the distribution in the CHBs has a peak around 20°. The peak may indicate that magnetic fields in CHBs have super radial structures or a converging structure toward the pole. Figure 14 is a scatter diagram of the horizontal (east–west) coordinates of the footpoint flares and the clockwise angles from the surface normal vector to the directions of the X-ray jets. If magnetic fields in CHBs have a super radial structure, most of the data points will be distributed in the second and fourth quadrants of the diagram. If most of the data points are distributed in the first and the third quadrants, it would mean that magnetic fields tend to converge toward the pole. Figure 14 shows that 71% of the data points are distributed in the second and fourth quadrants. We can therefore conclude that the magnetic fields in CHBs have a super radial structure.

4. SUMMARY AND DISCUSSION

We detected X-ray jets and transient brightenings around the north pole and in quiet regions near the equatorial limbs. We carried out a statistical study of these events associating them with regions in the PCHs, CHBs, PQRs, and EQRs. We found the following results.

1. We detected 844 X-ray jets by visual inspection and 3553 transient brightenings using an automatic detection method around the north pole. Furthermore, we detected 55 X-ray jets and 258 transient brightenings in equatorial quiet regions near the limbs. Different thresholds for the excess of X-ray intensities were set for the X-ray jets and transient brightenings. We therefore selected 478 X-ray jets and 1174 transient brightenings around the north pole for analysis. We have also selected 48 X-ray jets and 82 transient brightenings in the EQRs near the limbs.
2. We investigated the occurrence rates of the X-ray jets and transient brightenings in the polar regions as a function of distance from the boundaries of coronal holes. These rates show that coronal active events in the polar coronal holes occur uniformly in space, while most of the coronal activity in the polar quiet regions occurs adjacent to and equatorward of the boundaries of the coronal holes.
3. The mean occurrence rate of X-ray jets in the CHBs is two to three times higher than that in the PCHs, PQRs, and EQRs. The mean occurrence rate of transient brightenings in the CHBs is eight times higher than that in the PCHs, PQRs, and EQRs.
4. No large differences in the measured physical parameters (e.g., length, lifetime) are found for both the X-ray jets and transient brightenings in the PCHs, CHBs, PQRs, and EQRs. The mean parameters for X-ray jets are as follows: the length is 2.7×10^4 km, the lifetime is 10 minutes, the velocity is 170 km s^{-1}, the width is 4×10^4 km, the area is 3.5×10^7 km^2, and the thermal energy is 7×10^{25} erg. The parameters for transient brightenings are as follows: the lifetime is 5 minutes, the area is 3.0×10^7 km^2, and the thermal energy is 8×10^{25} erg.
5. The distribution of the directions of the X-ray jets suggests: (1) magnetic fields are almost radial in PCHs, (2) magnetic fields in CHBs have a super radial structure, and (3) closed loops in PQRs are rather randomly oriented.

Based on these results, we discuss the acceleration of the fast solar wind and the difference in occurrence rates of events among the polar regions in the following subsections.

4.1. Fast Solar Wind Acceleration by X-Ray Jets in PCHs

PCHs are thought to be the source region of the fast solar wind and we have also found that these regions frequently produce energetic X-ray jets. Cirtain et al. (2007) pointed out that polar X-ray jets may contribute to the fast solar wind because there are so many of them. Additionally, the apparent velocity of the outflows is very high. Furthermore, the unsigned angle distribution of the PCHs in Figure 13 shows that most X-ray jets in the PCHs erupted along open field. These facts suggest that X-ray jets in open field regions in PCHs may contribute to the acceleration of the fast wind.

We have estimated the thermal energy content in a thin X-ray jet structure. Our estimation is based on the results of Shimojo & Shibata (2000), who derived the temperatures and densities

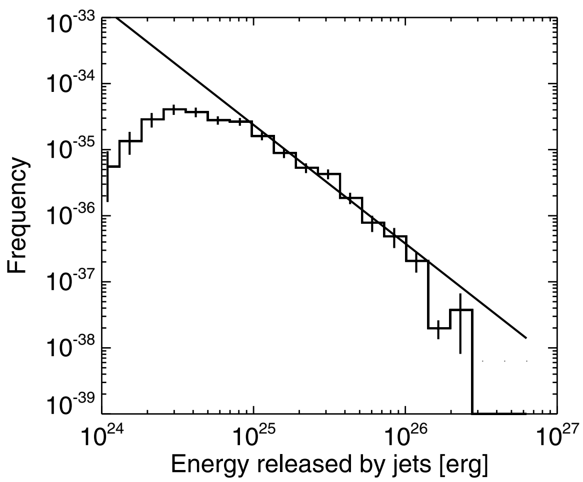

Figure 15. Frequency distribution as a function of the energy released by X-ray jets in the PCHs.

of X-ray jets that occurred in active regions using filter ratio analysis. The thermal energy of a typical footpoint flare was estimated by Shimojo & Shibata (2000) to be four to seven times as large as that of the thin structure. The thermal energy of the thin structure is on average three times larger than the kinetic energy. Therefore, we assume that the thermal energy of the thin structure is 1/4 that in the footpoint flare and the kinetic energy of the thin structure is 1/12 that of the footpoint flare. Using these estimates, we derive the total energy released by X-ray jets in the PCHs as the sum of the estimated thermal and kinetic energies of the thin structures. In this study, the thermal energy of a footpoint flare is measured at the time of its peak intensity. The time of the peak intensity in the footpoint flare, in most X-ray jets, is roughly consistent with the time when the X-ray jet's length is at its maximum. Therefore, our estimation of the energy released by X-ray jets is at the time of the maximum length.

From Figure 15, the distribution of the energy released by X-ray jets in the PCHs is a power law with an index of -1.79 ± 0.12, which is flatter than -2. If this distribution and power-law index remain valid between 10^{22} erg (nanoflare) and 10^{27} erg, we can derive 10^3 erg cm^{-2} s^{-1} as the upper limit of the total energy supplied by X-ray jets in the PCHs. Wang et al. (1996) estimated the energy flux of the solar wind to be more than 10^5 erg cm^{-2} s^{-1}. Even if X-ray jets directly become solar wind outflow, our PCHs' value suggests that they are not sufficiently energetic to explain the fast wind.

Neugebauer (2012) proposed that polar X-ray jets are the sources of microstream peaks in the fast solar wind. Microstream peaks exhibit velocity fluctuations of ± 35 km s^{-1}. Fluctuations of the energy flux by these velocity variations are estimated to be lower than 1% of the total energy flux, i.e., 10^3 erg cm^{-2} s^{-1}, as kinetic energy is thought to dominate the total energy flux of the fast solar wind. Polar X-ray jets therefore can supply sufficient energy to produce these velocity fluctuations in microstream peaks.

Shimojo & Shibata (2000) did not include the contribution of waves and Alfvénic flows in PCHs later discovered by Cirtain et al. (2007). We could not detect any evidence of waves or Alfvén flows because of the poor time cadence of our observations. However, reconnection models of X-ray jets suggest that the thermal energy of a footpoint flare is the dominant source of the energy provided to the entire X-ray jet, and the thin structure contains only a quarter of the total energy. Therefore, the contribution by waves and flows could be far less than these values.

4.2. Difference in Occurrence Rates of Transient Brightenings between the Regions

The mean occurrence rate of transient brightenings in the CHBs has been found to be higher than that in the PCHs, PQRs, and EQRs. Following previous studies (e.g., Shimizu et al. 2002; Huang et al. 2012) on the relationship between transient brightenings and emerging or canceling flux, we tried to estimate the occurrence rates of transient brightenings from those of flux emergence of cancellation events.

Iida et al. (2012) showed that the occurrence rate of flux emergence events was 1.2×10^{-10} km^{-2} hr^{-1} and that of flux cancellation events was 3.5×10^{-9} km^{-2} hr^{-1} in quiet regions. A few papers (Zhang et al. 2006; Abramenko et al. 2006; Hagenaar et al. 2008) reported that the occurrence rate of flux emergence events in coronal holes was less than half of that in quiet regions. Based on these results, we estimate the ratios of occurrence rates in the photosphere as follows: flux emergence in coronal holes to flux emergence in quiet regions to flux cancellation in quiet regions = 1:2:60. Note, however, that we actually need the rate of flux emergence to the height of the corona, not the photosphere, because transient brightenings occur in the corona. Some authors (e.g., Martínez González & Bellot Rubio 2009; Wiegelmann et al. 2010) have tried to evaluate the rate of events that reach the corona. However, their investigations were limited to quiet regions. Assuming that the difference in this rate is not significant between regions, our estimate for the ratios of the flux emergence/cancellation rates in the photosphere could also be applied to the coronal ratios.

The likelihood that magnetic fields will be involved in the coronal interaction may depend on the magnetic configuration in each coronal region. In PCHs, a single magnetic polarity is dominant except during solar maximum. Therefore, most of the open fields have the same polarity and closed loops rarely reach the corona, except by flux emergence (Shimojo & Tsuneta 2009). Assuming this to be the case, we can infer that transient brightenings in PCHs are caused only by flux emergence. On the other hand, quiet regions are filled with magnetic loops, and the polarity of the magnetic fields is balanced. Therefore, transient brightenings in PQRs and EQRs may be caused by magnetic interactions between emerging flux and existing coronal loops or between two coronal loops that are identified as canceling flux.

The magnetic environment in CHBs is not well known. However, we speculate that CHBs may have intermediate properties between coronal holes and quiet regions. Let us assume, therefore, that the situation with transient brightenings in CHBs is a mixture of those in PCHs and in PQRs/EQRs.

With these assumptions, however, the ratios of the occurrence rates of transient brightenings in the regions would be PCHs:CHBs:PQRs (EQRs) = 1:31.5:62, if the entire CHB area is equally divided between CH-like areas and QR-like areas. This is not consistent with our results, in which the occurrence rate in the CHBs exceeds the PQRs/EQRs rates.

It is interesting to note that the region with enhanced X-ray jet and transient brightening activity extends equatorward of the boundary beyond a distance of 10^5 km, although no contribution from active regions was recognized in the northern hemisphere as solar activity was very low in 2007 September. A possible scenario is that transient brightenings in CHBs are enhanced by interchange reconnection. Kahler et al. (2010) introduced a model suggesting that interchange reconnection could operate to maintain the quasi-rigid rotation of the boundaries of coronal holes against eastward photospheric convective motions. Fisk (2003) originally proposed the idea of interchange reconnection around the boundaries of coronal holes as a results of photospheric convective motions. These models present magnetic reconnection around the boundaries of coronal holes as a result of canceling flux in CHBs, but they cannot explain our result that extended CHB regions enhance the occurrence of X-ray jets and transient brightenings. One possibility is that our assumption that the rate of flux emergence to significant heights is uniform all over the solar surface may be too simplistic. A more detailed understanding of magnetic evolution from below the photosphere to high up in the corona is needed. Shimojo & Tsuneta (2009) presented the relationship between flux emergence and X-ray jets in the PCH region with only a very limited data set. We need further detailed statistical studies using more comprehensive data sets to clarify the relationship between activity in the corona and magnetic fields in the photosphere.

The authors thank Dr. David H. Brooks for editing the English text of our paper. This work was carried out at the NAOJ Hinode Science Center, which is supported by the Grant-in-Aid for Creative Scientific Research "The Basic Study of Space Weather Prediction" from MEXT, Japan (Head Investigator: K. Shibata), generous donations from Sun Microsystems, and NAOJ internal funding. *Hinode* is a Japanese mission developed and launched by ISAS/JAXA, collaborating with NAOJ as a domestic partner, NASA and STFC (UK) as international partners. Scientific operation of the *Hinode* mission is conducted by the *Hinode* science team organized at ISAS/JAXA. This team mainly consists of scientists from institutes in the partner countries. Support for the post-launch operation is provided by JAXA and NAOJ (Japan), STFC (UK), NASA, ESA, and NSC (Norway).

REFERENCES

Abramenko, V. I., Fisk, L. A., & Yurchyshyn, V. B. 2006, ApJL, 641, L65
Aschwanden, M. J., & Parnell, C. E. 2002, ApJ, 572, 1048
Aschwanden, M. J., Tarbell, T. D., Nightingale, R. W., et al. 2000, ApJ, 535, 1047
Canfield, R. C., Reardon, K. P., Leka, K. D., et al. 1996, ApJ, 464, 1016
Chifor, C., Isobe, H., Mason, H. E., et al. 2008, A&A, 491, 279
Cirtain, J. W., Golub, L., Lundquist, L., et al. 2007, Sci, 318, 1580
Fisk, L. A. 2003, JGRA, 108, 1157
Freeland, S. L., & Handy, B. N. 1998, SoPh, 182, 497
Golub, L., Deluca, E., Austin, G., et al. 2007, SoPh, 243, 63
Hagenaar, H. J., De Rosa, M. L., & Schrijver, C. J. 2008, ApJ, 678, 541
Huang, Z., Madjarska, M. S., Doyle, J. G., & Lamb, D. A. 2012, A&A, 548, A62
Iida, Y., Hagenaar, H. J., & Yokoyama, T. 2012, ApJ, 752, 149
Kahler, S., Jibben, P., & Deluca, E. E. 2010, SoPh, 262, 135
Kano, R., Sakao, T., Hara, H., et al. 2008, SoPh, 249, 263
Kosugi, T., Matsuzaki, K., Sakao, T., et al. 2007, SoPh, 243, 3
Kotoku, J., Kano, R., Tsuneta, S., et al. 2007, PASJ, 59, 735
Martínez González, M. J., & Bellot Rubio, L. R. 2009, ApJ, 700, 1391
Moreno-Insertis, F., Galsgaard, K., & Ugarte-Urra, I. 2008, ApJL, 673, L211
Narukage, N., Sakao, T., Kano, R., et al. 2011, SoPh, 269, 169
Neugebauer, M. 2012, ApJ, 750, 50
Nishizuka, N., Shimizu, M., Nakamura, T., et al. 2008, ApJL, 683, L83
Ogawara, Y., Takano, T., Kato, T., et al. 1991, SoPh, 136, 1
Savcheva, A., Cirtain, J., Deluca, E. E., et al. 2007, PASJ, 59, 771
Shibata, K., Ishido, Y., Acton, L. W., et al. 1992, PASJ, 44, L173
Shimizu, T. 1995, PASJ, 47, 251
Shimizu, T., Shine, R. A., Title, A. M., Tarbell, T. D., & Frank, Z. 2002, ApJ, 574, 1074
Shimojo, M., Hashimoto, S., Shibata, K., et al. 1996, PASJ, 48, 123
Shimojo, M., & Shibata, K. 2000, ApJ, 542, 1100
Shimojo, M., Shibata, K., & Harvey, K. L. 1998, SoPh, 178, 379
Shimojo, M., & Tsuneta, S. 2009, ApJL, 706, L145
Subramanian, S., Madjarska, M. S., & Doyle, J. G. 2010, A&A, 516, A50
Tsuneta, S., Acton, L., Bruner, M., et al. 1991, SoPh, 136, 37
Wang, Y.-M., Hawley, S. H., & Sheeley, N. R., Jr. 1996, Sci, 271, 464
Wiegelmann, T., Solanki, S. K., Borrero, J. M., et al. 2010, ApJL, 723, L185
Yang, S., Zhang, J., Li, T., & Liu, Y. 2011, ApJL, 732, L7
Yokoyama, T., & Shibata, K. 1995, Natur, 375, 42
Yokoyama, T., & Shibata, K. 1996, PASJ, 48, 353
Zhang, J., Ma, J., & Wang, H. 2006, ApJ, 649, 464